ORIGINAL PAPER

Low-temperature magnetic behavior of isocubanite from seafloor hydrothermal deposits in the Okinawa Trough

Chie Kato[1] · Masao Ohno[1] · Tadahiro Hatakeyama[2] · Yasuhiro Yamada[3] · Fuminori Honda[4] ·
Kazuhiko Shimada[5] · Toshiro Nagase[6] · Shuhei Totsuka-Shiiki[7,8] · Yoshihiro Kuwahara[1] · Jun-ichiro Ishibashi[5,9]

Abstract

The characteristic behavior of magnetic remanence correlated with mineralogical textures and composition was observed using low-temperature magnetometry, microscopy, and chemical analysis of three isocubanite samples collected from hydrothermal deposits in the Okinawa Trough and a sample transformed from natural cubanite via heating. Both zero-field remanence acquired at 5 K and field cooling remanence acquired at 300–5 K of all samples sharply decreased with increasing temperature at approximately 100 K. In addition, low-temperature cycling of isothermal remanence at 300 K exhibited a transition at approximately 100 K; remanence increased with decreasing temperature and vice versa. The intensity of remanence at low temperature and sharpness of the transition varied across samples with different compositions and microscopic textures, that is, the presence or absence of chalcopyrite lamellae and their widths. The sample obtained from a hydrothermal chimney, in which the magnetic transition was most clearly observed, was also subjected to X-ray diffraction, Mössbauer spectroscopy, electrical resistivity, and magnetic hysteresis measurements. The obtained results were generally consistent with those reported previously for unnamed mineral $CuFe_3S_4$ with an ordered cation arrangement. The low-temperature magnetic behavior of isocubanite possibly depends on the degree of cation ordering and can be regarded as an indicator of chemical composition and cooling history. Therefore, low-temperature magnetometry is useful for the detection of isocubanite and a potentially powerful technique for the prompt estimation of its composition and texture, contributing to our understanding of the formation process of hydrothermal deposits.

Keywords Isocubanite · Low-temperature magnetometry · Magnetic transition · Seafloor hydrothermal deposits

✉ Chie Kato
c.kato@scs.kyushu-u.ac.jp

1 Faculty of Social and Cultural Studies, Kyushu University, Fukuoka, Japan

2 Institute of Frontier Science and Technology, Okayama University of Science, Okayama, Japan

3 Department of Chemistry, Tokyo University of Science, Tokyo, Japan

4 Central Institute of Radioisotope Science and Safety, Kyushu University, Fukuoka, Japan

5 Faculty of Science, Kyushu University, Fukuoka, Japan

6 The Tohoku University Museum, Tohoku University, Sendai, Japan

7 Geological Survey of Japan, National Institute of Advanced Industrial Science and Technology, Tsukuba, Japan

8 Sumitomo Metal Mining Co., Ltd., Tokyo, Japan

9 Kobe Ocean-Bottom Exploration Center, Kobe University, Kobe, Japan

Introduction

Recent geological surveys have revealed seafloor massive sulfide (SMS) deposits, which have attracted attention as novel mineral resources. To explore the target areas of unknown ore deposits, geoscientific model of the formation process related to hydrothermal activity must be established. As SMS deposits are considered modern analogs of volcanic massive sulfide deposits (VMSDs), similar mineralogical studies have been conducted. To obtain constraints on the history of temperature and chemical conditions, sulfur fugacity, mineral assemblages, chemical composition of individual minerals, and microstructure of ore deposits have been investigated (e.g., Schwartz 1927; Mozgova et al. 2005; Fouquet et al. 2018; Fan et al. 2021).

Copper is not only an important industrial target but also a key element in understanding the history of sulfide ore deposits, as it forms various minerals that reflect the

environment. As some of the metal sulfides in the Cu–Fe–S system exhibit characteristic magnetic properties, the rock magnetic approach can provide information on the mineral species, composition, and texture of the constituent minerals through rapid and non-destructive measurements (e.g., Pearce et al. 2006). In particular, low-temperature magnetic analysis is expected to be effective for samples from hydrothermal deposits, which are vulnerable to severe alteration by heating, and useful for detecting minerals that are paramagnetic at room temperature but undergo magnetic transitions at low temperatures.

In the present study, we focus on isocubanite, which is specific to active seafloor hydrothermal fields (e.g., Mozgova et al. 2005). Isocubanite (stoichiometric formula $CuFe_2S_3$) is a high-temperature polymorph of cubanite, stable at > 210–270 °C (e.g., Sawada et al. 1962; Yund and Kullerud 1966; Fleet 1970; Cabri 1973; Putnis 1977). In the literature, isocubanite is often referred to as "intermediate solid solution (iss)" owing to the wide compositional range of the Cu–Fe–S ternary system at high temperatures (Caye et al. 1988). Isocubanite has a sphalerite-type face-centered cubic lattice structure, with Cu and Fe atoms randomly distributed at the cation sites (e.g., Fleet 1970; Szymański 1974; Lyubutin et al. 2015; Barbier et al. 2017, 2021).

Isocubanite can be obtained by heating natural cubanite in vacuum (e.g., Sawada et al. 1962; Fleet 1970; Putnis 1977) in the laboratory. This reaction is a structural transformation from orthorhombic to cubic as well as an order–disorder transition of the cation atoms. The transition is irreversible, and the metastable isocubanite can be quenched at ~ 25 °C. When annealed at temperature slightly lower than 200 ℃, fine lamellae of chalcopyrite emerge while the matrix remains disordered (Putnis 1977). According to Putnis, in metastable isocubanite, cation ordering within the cubic structure occurs instead of transition from isocubanite to cubanite, which is very sluggish at temperature as low as ~ 200 ℃. This reaction results in an overall reduction in free energy. Since the ordered cation occupancy of Cu:Fe = 1:2 is not geometrically feasible in the cubic lattice system, isocubanite breaks into chalcopyrite ($CuFeS_2$) and unnamed mineral ($CuFe_3S_4$). The decomposition of cubanite upon heating to a very fine mixture of chalcopyrite and a cubic phase, with X-ray powder diffraction pattern very similar to that of chalcopyrite, was also reported by Kaneda et al. (1978). Lamellae of isocubanite and chalcopyrite are often found in natural samples (e.g., Koski et al. 1984; Oudin et al. 1984; Zierenberg et al. 1984; Caye et al. 1988; Kase et al. 1990; Fouquet et al. 2018; Butler et al. 1998).

The magnetism of isocubanite is complex. The Mössbauer spectrum of cubic cubanite (isocubanite) is not magnetically split at 295 K, while it shows the evidence of magnetic ordering at low temperatures but cannot be resolved into simple sextet spectra. This complexity is explained by the randomness of the occupancy of cation sites by Fe^{2+}, Fe^{3+}, and Cu^{1+} ions (Greenwood and Whitfield 1968). Synthesized isocubanite shows paramagnetic behavior (Lyubutin et al. 2015; Barbier et al. 2017; 2021).

Wintenberger et al. (1994) reported the magnetic structure and transition of unnamed mineral $CuFe_3S_4$ with chalcopyrite exsolution collected from the Snake Pit hydrothermal field (Mid-Atlantic Ridge at 23° N). They reported that their sample showed ordered cation occupancy and a tetragonal crystal structure, in which the sphalerite-type cubic lattice of isocubanite is slightly distorted. Hereafter, the abbreviations *cp* for chalcopyrite and *np* ('new phase') for $CuFe_3S_4$ are used, following Wintenberger et al. (1994). They also reported that upon cooling, three magnetic transitions were observed in np at approximately 285, 190, and 105 K. Moreover, a magnetic transition occurs below ~ 105 K, where np becomes ferrimagnetic, and its magnetic moment and electric resistivity increase dramatically. Since the chemical compositions and crystal structures of $CuFe_3S_4$ and isocubanite are very close to each other, isocubanite with intermediate compositions may exhibit similar magnetic properties. In particular, it may be a useful indicator for isocubanite if a characteristic magnetic transition is recognized upon low-temperature magnetometry.

In the present study, using X-ray diffraction (XRD) measurements, magnetic analyses, Mössbauer spectroscopy, electrical resistivity measurements, and chemical analysis, we investigated the magnetic properties of isocubanite samples collected from submarine hydrothermal deposits in the Okinawa Trough and a sample obtained in the laboratory by heating natural cubanite.

Sample description

Stoichiometric isocubanite obtained by transition from cubanite

To obtain a stoichiometric isocubanite sample, a cubanite sample from the Henderson No. 2 mine, Chibougamau, Quebec, Canada, was heated using the Curie Balance (NMB-2000M1, Natsuhara Giken) in vacuum (< 10 Pa). The change in the magnetization of the sample was monitored during heating and cooling to confirm the transition from ferromagnetic cubanite to paramagnetic isocubanite. The thermomagnetic (Js-T) curve is presented in Fig. 1. The magnetization of cubanite was almost constant up to 250 °C and drastically decreased at 250–280 °C due to phase transition to isocubanite. The mass-specific magnetization of the sample in 300 mT before and after heating was approximately 0.4 Am^2 kg^{-1} and 0.005 Am^2 kg^{-1}, respectively. The Js–T curve was irreversible, suggesting that the inverse transition from isocubanite to cubanite did not occur upon cooling to
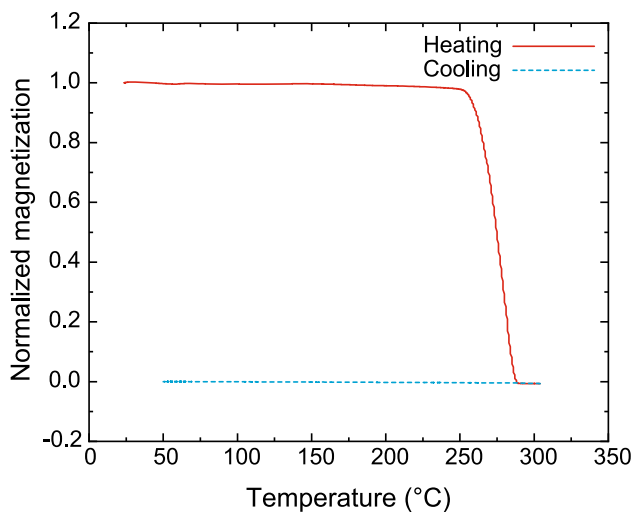
Fig. 1 Thermomagnetic (Js–T) curve of cubanite/isocubanite in 300 mT. Red solid line and blue dashed line indicate heating and cooling curves, respectively

room temperature. No signals indicating the formation of other magnetic minerals, such as magnetite, were detected. The phase transition from cubanite to isocubanite was also confirmed by XRD measurements before and after heating (see the next section). Hereafter, this sample is referred to as sample #1.

Isocubanite samples from the Okinawa Trough

Natural isocubanite samples (samples #2, #3, and #4) were obtained from active seafloor hydrothermal fields in the Okinawa Trough during research cruises under the framework of the Next-Generation Technology for Ocean Resources Exploration Project, Cross-Ministerial Strategic Innovation Promotion Program (SIP) of the Japanese Cabinet Office (e.g., Nozaki et al. 2021). The Okinawa Trough is a back-arc basin of the Ryukyu Trench–Arc system, located along the eastern coast of the Eurasian continent. The tectonic setting of the Okinawa Trough is considered to be in the rifting stage, in which the extension of the lithosphere with a normal fault system is dominant. More than ten hydrothermal fields are located in the Okinawa Trough, and sulfide deposits associated with hydrothermal activities have attracted attention as modern analogs of Kuroko-type ore deposits (e.g., Halbach et al. 1989; Ishibashi et al. 2015).

Isocubanite sample #2 was obtained from a sediment core obtained by scientific drilling at the Noho Site near the Iheya Small Ridge. Drilling was conducted during the CK16-01 Cruise (Exp. 908) of D/V *Chikyu* in 2016, and the drilled site (Site C9017) was located near active hydrothermal chimneys that vigorously emanated high-temperature (> 330 °C) fluids. The drilled cores from Site C9017 primarily comprised

basaltic lava, altered volcanic rocks, and clays. Isocubanite sample #2 was collected from a core sample labeled C9017C-11H-1W, 65.0–68.0 cm, obtained at 71.650 mbsf. A small amount of sulfide minerals was recognized within altered rock fragments. Based on onboard XRD, optical microscopic observations, and EPMA analysis, the constituent minerals were pyrrhotite, anorthite, chlorite, (iso)cubanite, titanite, and K-feldspar (Totsuka 2017).

Isocubanite sample #3 was obtained from a sediment core by scientific drilling at the Hakurei Site in the Izena Hole. Drilling was conducted during the CK16-05 Cruise (Exp. 909) of D/V *Chikyu* in 2016. The drilled site (Site C9026) was in the vicinity of the Northern Mound, a few tens of meters high. The drilled cores from Site C9026 comprised pumiceous sediments at the top, a sulfide body dominated by pyrite, marcasite, and sphalerite/wurtzite, and underlying hydrothermally altered clay. Isocubanite sample #3 was collected up from a core sample labeled C9026A-13X-1W, 20.0–23.0 cm, obtained at 74.700 mbsf. According to onboard core description (Nozaki et al. 2021), this depth was within hydrothermally altered clay that contains veins of pyrrhotite and isocubanite located 10–15 m beneath the sulfide body.

Isocubanite sample #4 was obtained from a fragment of an active chimney at the Noho Site. The chimney fragment was collected by the ROV *Hyper-Dolphin* during the NT15-13 Cruise of R/V *Natsushima* in 2015 and labeled HPD1860R05(4). The distance between the sampling points and Site C9017 was within a few tens of meters. The chimney fragment is composed of anhydrite and sulfides, such as isocubanite, sphalerite, pyrrhotite, and pyrite (Totsuka 2017). Isocubanite grains as large as a few centimeters in diameter were observed in the polished section. High-resolution optical and electronic microscopy and chemical analyses revealed that it consisted of fine lamellae of Fe-rich isocubanite and Fe-rich chalcopyrite.

From the core samples, fragments of aggregated sulfides were selected, freeze-dried, and crushed to collect pieces, including isocubanite, under a binocular microscope. Unfortunately, the isocubanite grain size in samples #2 and #3 was very small, and these samples could not be obtained without contamination.

Sample #4 was prepared as follows. First, a chimney body sample was crushed using a mortar and pestle. Then ferromagnetic particles, such as pyrrhotite, were removed using a neodymium magnet. Finally, the particles without surface staining were selected under a binocular microscope.

Methods

Powder XRD measurements were conducted on samples #1 and #4 using a benchtop X-ray diffractometer (Rigaku, MiniFlex II, Cu-Kα) at Kyushu University. The results

were analyzed and fitted using the PDXL2 software built into the diffractometer and the PDIndexer software by Seto et al. (2010).

For all samples, a series of low-temperature magnetic measurements commonly adopted in rock magnetic studies were conducted as follows. In low-temperature remanence measurements, isothermal remanent magnetization (IRM) was first imparted to the sample by a DC field of 5 T at 5 K after zero-field cooling from 300 K. Next, remanent magnetization was measured during warming to 300 K in a zero field (ZFC remanence). Subsequently, the sample was cooled again to 5 K in a 5 T field, and remanence was measured during warming in a zero field (FC remanence). The sample was then exposed to 5 T at 300 K, and IRM was measured during cooling to 5 K and heating to 300 K in zero field. Magnetization was measured at 2.5–5.0 K intervals in the sweep mode of 2.5–5.0 K/min. Additional measurements were conducted on sample #4 to directly compare the results with those reported by Wintenberger et al. (1994) for np ($CuFe_3S_4$). After low-temperature remanence measurements, the sample was demagnetized by switching the direction of the applied DC field, which decays stepwise from 5 T to zero field, and its magnetization was measured in a DC field of 150 mT during cooling and warming between 300 and 5 K. Hysteresis measurements were conducted at 77, 130, 200, and 300 K with applied maximum field of 5 T. The field increment was 10 mT between -100 mT and + 100 mT, and 100 mT beyond this range. All magnetic measurements were performed using a magnetic property measurement system (MPMS-XL5, Quantum Design Inc.) at Okayama University of Science and Kochi University.

On sample #4, Mössbauer spectroscopy was performed at 293, 225, 120, and 3 K to compare the ^{57}Fe hyperfine magnetic structure with that reported by Wintenberger et al. (1994). Isocubanite grains were hand-picked under a binocular microscope, coarsely ground using a mortar and pestle, and subjected to measurements. Mössbauer spectroscopy was performed at RIKEN using a Mössbauer Drive Unit (MDU1200, Wissel) with a ^{57}Co/Rh radiation source. The electrical resistivity of sample #4 was measured using the conventional four-probe AC method with a physical property measurement system (PPMS, Quantum Design Inc.) starting from 2 K at IMR, Tohoku University. Resistivity was measured during both cooling and heating.

After the above analyses, all samples were mounted in epoxy resin and polished for microscopic observation and chemical analysis. A field-emission electron probe micro-analyzer (FE-EPMA, JEOL) at Kyushu University was used to analyze the chemical composition of isocubanite and other sulfide minerals. An accelerating voltage of 15 kV and a beam current of 5 nA were used. The electron beam was usually 5 μm in diameter but focused to 1 μm when

measuring exsolved phases. The counting time for each element was 40 s.

Results

XRD measurements

One-dimensional XRD profiles of samples #1 and #4 are shown in Fig. 2. The crystal structure and lattice constant of sample #1 were consistent with those of stoichiometric isocubanite ($CuFe_2S_3$) reported in the literature (Szymański 1974), indicating that cubanite was successfully transformed into isocubanite.

The XRD profile of sample #4 was generally consistent with that of isocubanite; however, the peak positions of some of the diffraction lines appeared at a slightly smaller d. We fitted the structure of np ($CuFe_3S_4$) with the space group I-42 m proposed by Wintenberger et al. (1994) to this profile and obtained the lattice constants of $a = 5.3028(8)$ and $c = 10.6100(20)$ Å, which are slightly smaller than those of np. Although Mössbauer spectroscopy and microscopic observations described later suggest the existence of chalcopyrite, it was not apparent from the XRD profile because the crystal structures of np and chalcopyrite are very similar and the diffraction lines can overlap. Deviation from a bell-shaped distribution at diffraction lines 112, 204, and 312 of np was interpreted to be due to chalcopyrite, which should appear at a slightly larger 2θ than that of np (insets in Fig. 2). This deviation was not observed for sample #1.

Magnetic measurements

The results of low-temperature remanence measurements are shown in Fig. 3. Note that the magnetizations are plotted in a logarithmic scale. In all studied samples, the magnetization changed significantly at approximately 100 K. The strengths of the ZFC and FC remanences acquired at 5 K decreased monotonically with increase in temperature, with the sharpest decrease at approximately 100 K. The decrease in remanence was much smaller at > 100 K. IRM was weak at 300 K but increased sharply at ~ 100 K during the cooling process; this change was almost reversible upon heating to 300 K.

The magnitude of remanence at low temperatures and sharpness of change at approximately 100 K differed among the samples. For example, the ZFC remanence was ~ 15 Am^2 kg^{-1} for sample #4, which was 70 times larger than that (~ 0.2 Am^2 kg^{-1}) for sample #1. One or two minor transitions at temperatures higher than 100 K were observed in samples #3 and #4 but not in samples #1 and #2. Contrary to the magnetization at temperatures below 100 K, the magnetization at 300 K was smallest in sample #4. Relatively large magnetization at 300 K in samples #1, #2, and #3 may be attributed
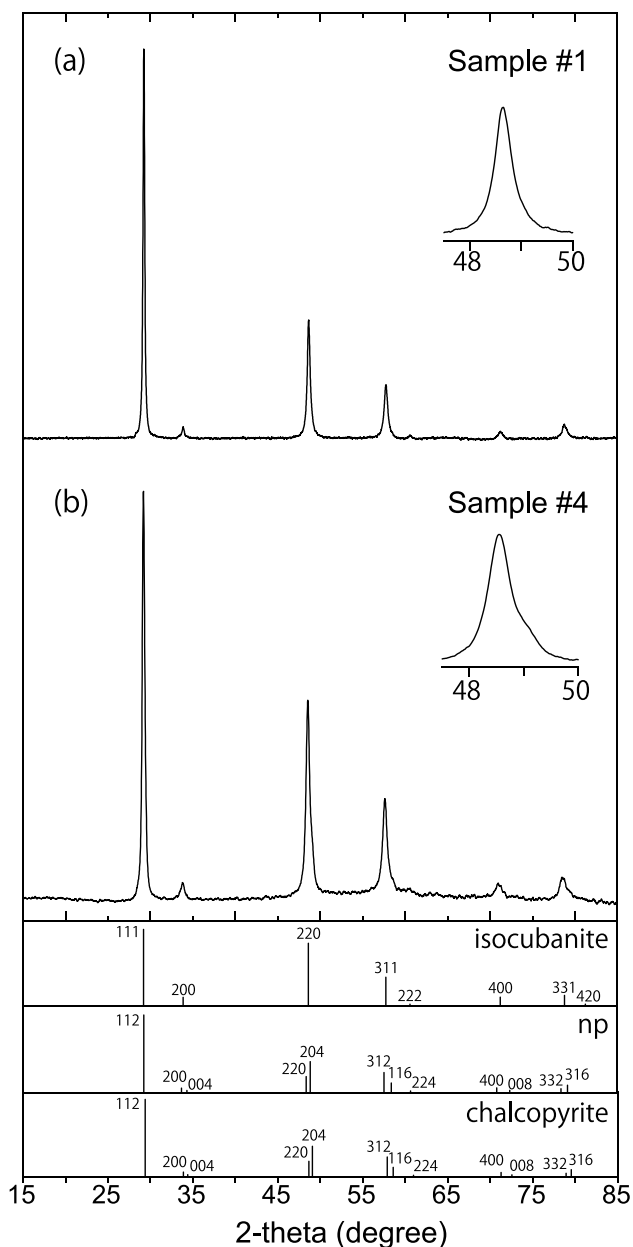
Fig. 2 One-dimensional X-ray diffraction profile of **a** sample #1 and **b** sample #4. The lower part of the figure shows the theoretical 2θ angle and intensities of the reflections of isocubanite, np, and chalcopyrite, calculated using VESTA (Momma and Izumi 2011)

to trace magnetic phase(s) resulting from heating of cubanite (sample #1) or in the matrix (samples #2 and #3).

The result of the low-temperature cycling in 150 mT on sample #4 is presented in Fig. 4. A major magnetic transition was observed at ~ 100 K, in which the magnetization increased with decreasing temperature below the transition point, similar to the remanence measurements. The saturation value of ~ 10 Am^2 kg^{-1} at 10 K was also similar to that (15 Am^2 kg^{-1}) reported by Wintenberger et al. (1994) for np.

The hysteresis loops measured at different temperatures are shown in Fig. 5a. At 77 K, it showed a hysteresis loop typical for ferromagnetic or ferrimagnetic materials with coercivity of 400 mT and saturation magnetization of 18 Am^2 kg^{-1} (Fig. 5b). The shape of the hysteresis loop was virtually identical to that reported by Wintenberger et al. (1994) for np. At 130 K, the magnetization at 5 T was about one-sixteenth of that at 77 K and the hysteresis loop showed magnetically harder nature that does not saturate even at 5 T. At 200 K, the shape of the hysteresis loop was close to those reported for antiferromagnetic materials (Cuda et al. 2011). At 300 K, the sample showed almost no hysteresis, and the magnetization at 5 T was the smallest among the measured loops.

## Mössbauer spectroscopy and electrical resistivity

The acquired Mössbauer spectra of sample #4 are shown in Fig. 6. The spectrum obtained at 293 K was fitted to a combination of paramagnetic doublets and sextets. The doublet and sextet were comparable to the np and cp values reported by Wintenberger et al. (1994) at 295 K, respectively. Although the two components of np (np1 and np2) were distinguished by Wintenberger et al. (1994), we could not separate them into two phases. The Mössbauer spectrum acquired at 225 K showed a combination of cp sextet, doublet, and sextet. The spectra acquired at 120 and 3 K were fitted to obtain three sets of sextets. The components fitted at 225, 120, and 3 K were interpreted to be identical to the signals of np1, np2, and cp reported by Wintenberger et al. (1994) at the corresponding temperatures, but the volume ratios of np and cp were different. The fitted Mössbauer parameters are listed in Table 1.

Electrical resistivity as a function of temperature is presented in Fig. 7. A clear anomaly in the resistivity was observed at ~ 100 K, where major transition in the temperature dependence of magnetization was observed. Resistivity showed a semiconductor-type temperature dependence below the transition temperature, where resistivity decreases with increasing temperature. Above this transition, resistivity increases with increasing temperature. Thermal hysteresis was observed, indicating the occurrence of first-order phase transition.

Microscopy and chemical analysis

Micrographs and backscattered electron (BSE) images are presented in Fig. 8, and the results of the chemical analyses are summarized in Table 2. In addition, the compositions of isocubanite and chalcopyrite lamellae were plotted on the Cu–Fe–S ternary diagram (Fig. 9). Sample #4 was characterized by micron-scale lamellae of relatively Fe- and Cu-rich phases. Bulk composition measured by the

Fig. 3 Low-temperature remanence *versus* temperature curves. **a** Sample #1. **b** Sample #2. **c** Sample #3. **d** Sample #4. Dashed and solid red bold lines represent ZFC and FC remanences, respectively. Dashed and solid blue lines indicate cooling and heating of 300 K-IRM, respectively
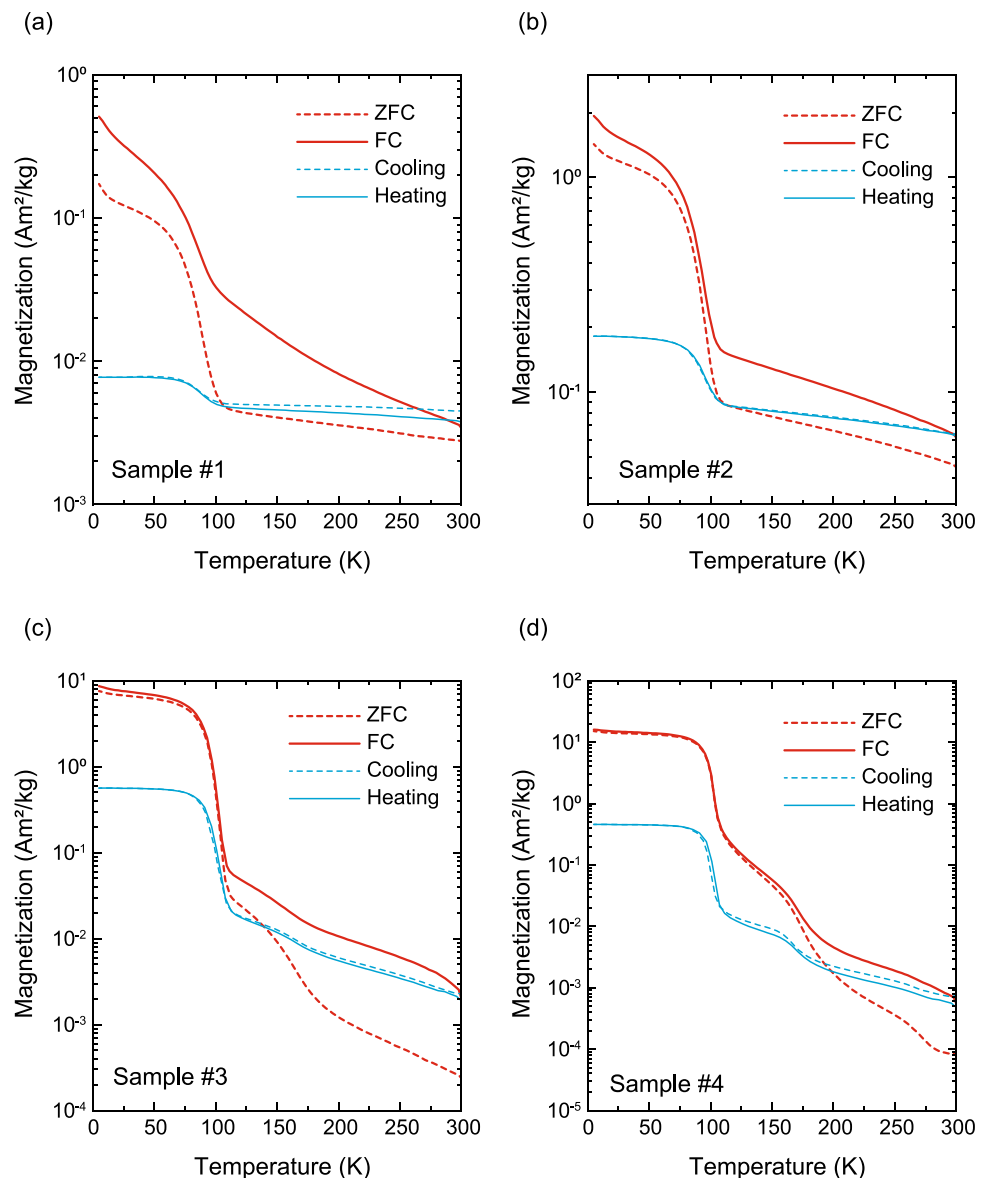
defocused electron beam was between that of stoichiometric isocubanite ($CuFe_2S_3$) and np ($CuFe_3S_4$). Although accurate measurements were not possible because of the small particle sizes, the Fe-rich phase was not expected to be as Fe-rich as that in np, and the Cu-rich phase was possibly chalcopyrite but rich in Fe. Similarly, sample #3 exhibited lamellae of Fe-rich isocubanite and chalcopyrite, but they were as wide as a few micrometers. This texture enabled us to analyze the composition of each phase separately. The composition of Fe-rich isocubanite in sample #3 was very close to the bulk composition of sample #4. Tiny spots of a Zn-rich phase, possibly sphalerite, were observed in Fe-rich isocubanite. In sample #2, chalcopyrite lamellae were not observed, but spots of pyrite were detected in the Fe-rich isocubanite. The composition of Fe-rich isocubanite was close to that in sample #3 and bulk composition in sample

#4 but was slightly more Cu-rich, close to the stoichiometric composition (Fig. 9). Sample #1 showed no inner structure, and its composition was close to $CuFe_2S_3$.

Discussion

Low-temperature magnetic transition of isocubanite

A magnetic transition at ~ 100 K was observed in all measured isocubanite samples, regardless of the texture or composition. Considering the variety in sample compositions, such a magnetic transition may be a general property of isocubanite within a certain composition range. The temperature dependence of magnetization and electrical resistivity
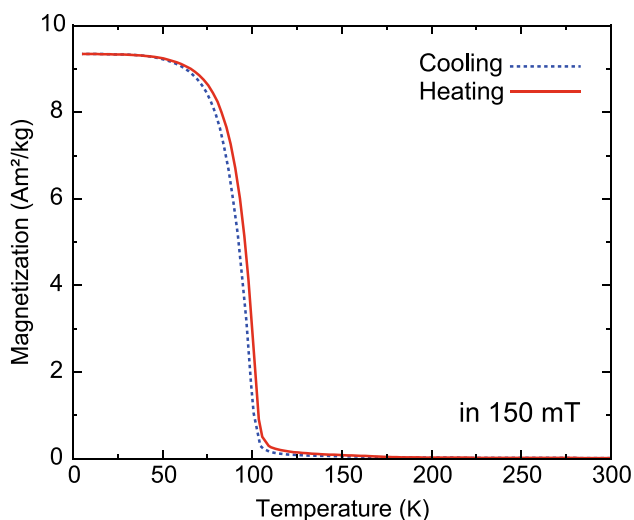
Fig. 4 Result of magnetization *versus* temperature in 150 mT for sample #4

in sample #4 resembled that in np reported by Wintenberger et al. (1994), who argued that it was a Verwey transition. The transition temperature of ~ 100 K and the decay of ZFC and FC remanences across the transition may mimic those of magnetite, a representative magnetic material that undergoes the Verwey transition (Özdemir et al. 1993; Moskowitz et al. 1993; Kosterov 2003). However, it can be clearly distinguished by the following points. First, the strength of the IRM acquired at 300 K increased with decreasing temperature at the transition, contrary to the case in magnetite. This

is possibly owing to the orientation of spontaneous magnetization by the weak magnetization carried by impurities and/or local magnetic regions. Second, the magnetization drop at the transition was as large as at least one order of magnitude. This implies large (> 100 μm) grain size in the case of magnetite, in which the ZFC remanence is considerably larger than the FC remanence (Kosterov 2003), contrary to our observation on the isocubanite samples. Moreover, the temperature dependence of the hysteresis loops shown in Fig. 5 implies that the nature of the transition in isocubanite is a ferrimagnetic/antiferromagnetic one, such as that reported for troilite at 70 K (Cuda et al. 2011), rather than a Verwey transition.

Comparison of sample #4 to the sample studied by Wintenberger et al. (1994)

The XRD spectra, low-temperature magnetic properties, electrical resistivity, and Mössbauer spectra of sample #4 were generally consistent with those of the sample studied and reported by Wintenberger et al. (1994). Although Wintenberger et al. (1994) did not show microscopic images, their described microstructure of "an orthogonal network of very thin (~ 0.5 μm) alternate lamellae" is also consistent with our observations (Fig. 8d, e). The similarity in the microstructure was further supported by the results of hysteresis measurements at 77 K, which are sensitive to magnetic grain size. However, the chemical composition was different; Wintenberger et al. (1994) noted that the bulk (np + cp) composition of their sample was very
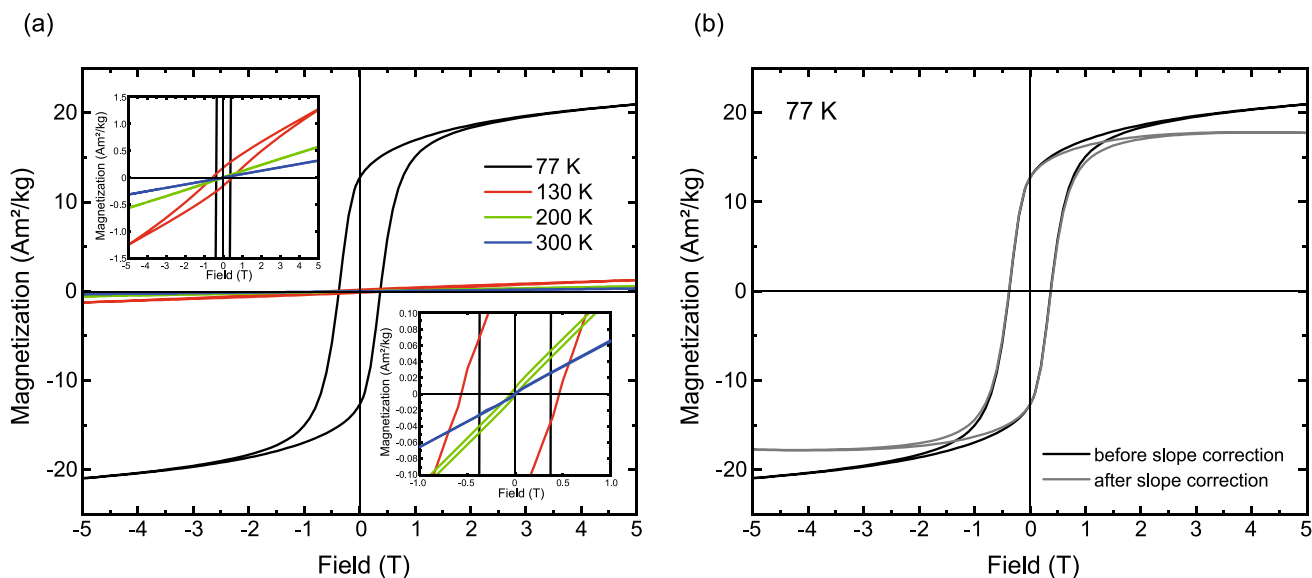
(a)

(b)

Fig. 5 Results of magnetic hysteresis measurements for sample #4. **a** Black, read, blue, and green lines are the hysteresis loops at 77, 130, 200, and 300 K, respectively. Insets show the magnified views near the origin. **b** Hysteresis loop at 77 K. Grey line shows the loop after the paramagnetic slope correction
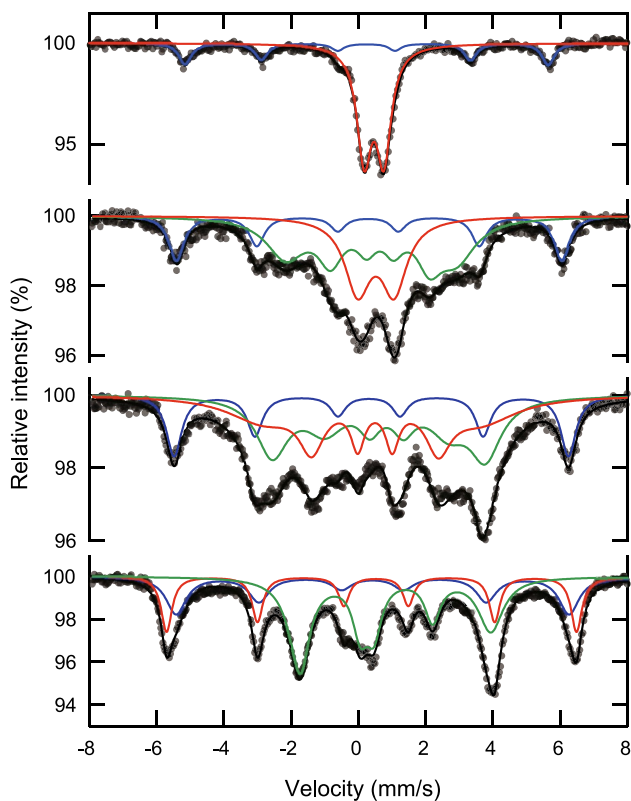
Fig. 6 Mössbauer spectra of sample #4 at **a** 293 K, **b** 225 K, **c** 120 K, and **d** 3 K. Green, red, and blue lines are the fitted sub-spectra corresponding to np1, np2, and cp, respectively

Fig. 7 Electrical resistivity *versus* temperature curve of sample #4. Closed black circles and open red circles indicate resistivity measured during cooling and heating, respectively. Inset is a magnified view near the transition

close to that of $CuFe_2S_3$, and np was slightly more Fe-rich than $CuFe_3S_4$. Meanwhile, sample #4 corresponded to $Cu_{1.8}Fe_{4.1}Zn_{0.1}S_6$ in bulk, and its Fe-rich isocubanite phase showed a lower Fe/Cu ratio than $CuFe_3S_4$ (Table 2). In addition, a difference in mineral composition can be
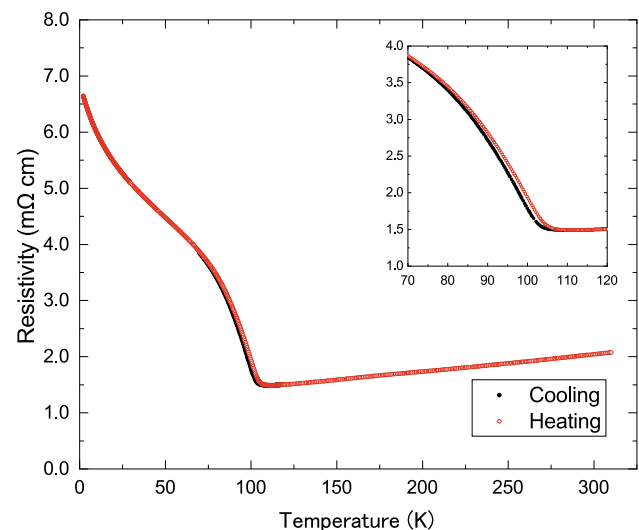
inferred from the relative contribution of each sub-spectrum to the Mössbauer spectra. Wintenberger et al. (1994) reported that ~40% of the Fe atoms belonged to cp, whereas our results indicated that only ~25% Fe atoms belonged to cp. Such differences in the chemical and mineral compositions may be due to the different histories of individual samples.

The difference in bulk composition indicated that the initial composition of isocubanite before decomposition was different, possibly reflecting its history at high temperatures, where the isocubanite/intermediate solid solution was stable. In addition, the differences in the ratio of

Table 1 Fitted ^{57}Fe Mössbauer parameters of sample #4

T	Site	d	DEq	H	G	P
K		mm s^{-1}	mm s^{-1}	T	mm s^{-1}	%
293	cp	0.24 (1)	0	33.4(1)	0.44 (3)	26
	np	0.44 (2)	0.58 (1)		0.52 (1)	74
225	cp	0.30 (1)	0	35.4 (1)	0.53 (3)	21
	np2	0.52 (1)	1.08 (2)		0.82 (4)	30
	np1	0.51 (1)	− 0.26 (2)	15.7 (1)	1.39 (6), 1.04 (8), 0.60 (4)	49
120	cp	0.35 (1)	0.06 (1)	36.3 (1)	0.54 (2)	21
	np2	0.45 (6)	− 0.07 (9)	20.1 (2)	2.6 (5), 0.9 (1), 0.5 (1)	38
	np1	0.72 (4)	− 0.25 (7)	19.6 (1)	1.1 (1), 1.4 (1), 0.8 (1)	41
3	cp	0.42 (1)	0	36.2 (2)	0.72 (4)	25
	np2	0.46 (1)	− 0.13 (1)	37.7 (1)	0.39 (2)	26
	np1	0.81 (1)	0.66 (1)	17.8 (1)	0.89 (3), 0.56 (3), 0.56 (3)	49

d isomer shift (ref. Fe metal), *ΔEq* quadrupole energy, *H* magnetic hyperfine field, *G* linewidth FWHM, *P* relative area of various sub-spectra, *cp* chalcopyrite, *np1, np2* sites 1 and 2 of $CuFe_3S_4$ from Wintenberger et al. (1994)

Fe-rich isocubanite (np) and Fe-rich chalcopyrite (cp) as well as the composition of each phase indicate how far the decomposition of isocubanite has progressed, which depends on history after the temperature drops below the stable range of isocubanite.

As shown in Fig. 3, at above ~ 100 K, magnetization decreases monotonically with increasing temperature; however, inflection points were observed at ~ 170 and ~ 250 K in sample #4. These changes possibly correspond to the transitions proposed by Wintenberger et al. (1994), although the temperature was slightly different, which can be attributed to the differences in chemical composition.

Overall, we conclude that sample #4 exhibits similar texture and undergoes qualitatively similar magnetic transitions at low temperatures to the sample described by Wintenberger et al. (1994), both produced by the decomposition of isocubanite at temperatures below its stability range. Subtle differences in chemical and mineral composition reflect the cooling history.

Linkage of magnetic properties, mineral composition, and texture

The strength of low-temperature magnetization, sharpness of transition at ~ 100 K, and presence/absence of minor transitions at high temperatures varied among the samples. This difference may be attributed to the variation in the degree of cation ordering; the most ordered case is np in which the ratio of Cu and Fe is 1:3, and the most disordered case is ideal isocubanite in which the ratio of Cu and Fe is 1:2. In this section, we discuss how the differences in magnetic properties among the samples can be explained by the chemical composition and microstructure.

Samples #3 and #4 exhibited strong magnetization at low temperatures; however, minor transitions at high temperatures were observed more clearly in sample #4. Further microscopic observations and chemical analysis revealed that sample #4 exhibited a lamellar structure on the order of one micrometer, while in sample #3, each phase was on the scale of a few to tens of micrometers. Moreover, the Fe-rich isocubanite phase in sample #4 showed a larger Fe/Cu ratio than that in sample #3. Therefore, the composition of Fe-rich isocubanite in sample #4 was closer to $CuFe_3S_4$ than that in sample #3; thus, more parts can contribute to the ordered structure of np, resulting in a clearer transition.

The low-temperature magnetization of sample #1 was the weakest among the studied samples; nonetheless, it was still significant, and the transition at ~ 100 K was also clear. Such a transition was not recognized in synthesized isocubanite (Lyubutin et al. 2015), although it is consistent with the report by Greenwood and Whitfield (1968) that
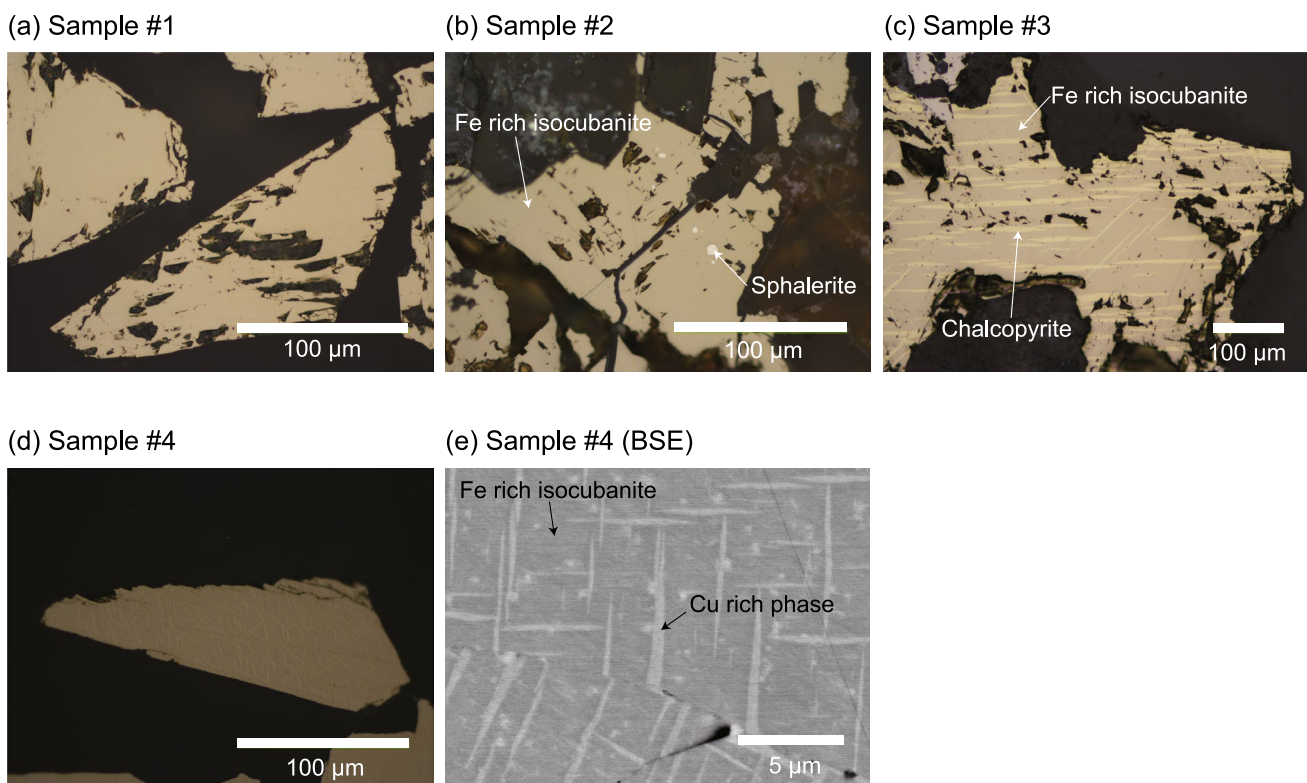

Fig. 8 Optical micrographs of **a** sample #1, **b** sample #2, **c** sample #3, and **d** sample #4, and **e** BSE image of sample #4

Table 2 Chemical compositions of isocubanite and chalcopyrite in samples #2, #3, and #4, as determined by EPMA

Sample	Composition (weight %)						
	Cu	Fe	Ni	Zn	Pb	S	Total
Sample #2	21.68	41.11	0.00	0.62	0.19	35.11	98.71
Fe-rich isocubanite	21.70	41.40	0.00	0.75	0.00	35.44	99.28
(no lamellae observed)	21.26	41.10	0.00	0.73	0.00	34.99	98.09
	21.15	41.36	0.03	0.62	0.00	34.78	97.93
	21.22	41.39	0.02	0.70	0.17	35.24	98.75
	21.70	41.54	0.00	0.66	0.11	34.62	98.62
	21.31	41.27	0.00	0.69	0.00	35.45	98.72
	21.33	41.72	0.00	0.63	0.09	34.91	98.68
Mean	21.42	41.36	0.01	0.68	0.07	35.07	98.60
SD	0.23	0.21	0.01	0.05	0.08	0.30	-
Sample #3	21.15	41.21	0.09	0.46	0.02	35.09	98.02
Fe-rich isocubanite	20.85	42.14	0.00	0.52	0.00	34.76	98.26
	21.42	42.29	0.02	0.77	0.06	34.78	99.35
	21.21	41.71	0.03	0.68	0.28	34.63	98.54
Mean	21.16	41.84	0.04	0.61	0.09	34.81	98.54
SD	0.24	0.49	0.04	0.14	0.13	0.20	-
Sample #3	30.06	33.37	0.01	0.17	0.00	34.36	97.97
Fe-rich chalcopyrite	31.09	33.33	0.03	0.15	0.00	33.39	97.99
	29.77	33.43	0.00	0.15	0.12	34.22	97.70
	30.38	32.31	0.00	0.28	0.16	34.63	97.75
	31.14	33.85	0.00	0.29	0.08	34.47	99.83
Mean	30.49	33.26	0.01	0.21	0.07	34.21	98.25
SD	0.61	0.57	0.01	0.07	0.07	0.48	-
Sample #4	20.81	41.04	0.00	1.35	0.00	34.50	97.70
(by defocused beam)	21.55	41.27	0.04	0.93	0.04	34.63	98.45
	22.17	41.00	0.05	0.93	0.04	34.23	98.42
	21.51	42.02	0.08	1.15	0.26	34.68	99.69
	20.33	41.82	0.01	1.13	0.04	35.09	98.43
	20.40	41.69	0.03	1.20	0.00	34.83	98.15
	20.24	41.77	0.00	1.24	0.22	34.30	97.77
	20.70	42.04	0.00	1.28	0.18	34.78	98.98
	19.99	42.05	0.11	1.34	0.12	34.53	98.15
	20.53	41.62	0.08	1.11	0.08	34.59	98.00
	20.32	42.23	0.00	1.03	0.18	34.53	98.30
	21.17	40.85	0.00	1.21	0.16	35.22	98.61
	20.67	41.70	0.00	1.24	0.14	34.80	98.55
Mean	20.80	41.62	0.03	1.16	0.11	34.67	98.40
SD	0.63	0.45	0.04	0.14	0.09	0.28	-
Sample #4	19.29	43.07	0.00	1.14	0.20	34.23	97.93
Fe-rich isocubanite	19.10	43.14	0.00	0.99	0.00	34.37	97.60
(lower limit of Fe/Cu)	19.66	43.75	0.00	0.96	0.00	34.26	98.63
Presumably contaminated by Cu-rich lamellae							
Mean	19.35	43.32	0.00	1.03	0.07	34.29	98.06
SD	0.29	0.37	0.00	0.09	0.12	0.07	-

the Mössbauer spectrum at low temperatures showed evidence of magnetic ordering. Although long-range ordering is absent because of the random occupancy of cation sites, local ordering of cations may be responsible for the weak magnetization of $CuFe_2S_3$ isocubanite.

Although the chemical compositions of the Fe-rich isocubanite phases of samples #2 and #3 were very similar
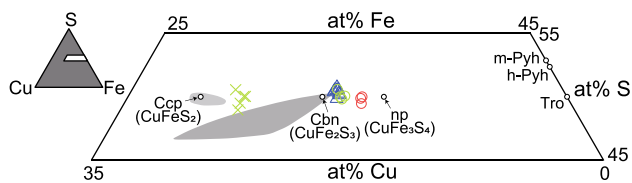
Fig. 9 Chemical composition of the studied samples plotted on the Cu–Fe–S ternary diagram. Inset shows the position of the magnified figure. Blue, green, and red represent samples #2, #3, and #4, respectively. Circles and crosses indicate Fe-rich isocubanite and chalcopyrite lamellae, and triangle indicates isocubanite without chalcopyrite lamellae. Stoichiometric compositions of the relevant phases are shown by small black opened circles; Cbn: cubanite (identical to stoichiometric isocubanite), Ccp: chalcopyrite, h-Pyh: hexagonal pyrrhotite, m-Pyh: monoclinic pyrrhotite, np: new phase (unnamed mineral $CuFe_3S_4$ described by Wintenberger et al. (1994), Tro: troilite. Areas painted in light and dark gray indicate chalcopyrite and isocubanite (intermediate) solid solutions at 350 °C, as reported by Sugaki et al. (1975)

and the fraction of Fe-rich isocubanite was higher in sample #2, magnetization of sample #3 was approximately five times that of sample #2. This difference was significant, although the samples were not completely separated from the matrix. Regarding mineral texture, chalcopyrite lamellae were detected in the Fe-rich isocubanite of sample #3 but not in that of sample #2. These differences in texture and magnetization can be explained as follows. At the temperature at which the disordered solid solution is metastable, the occurrence of ordering and/or decomposition is governed by kinetics, which are predominantly affected by temperature. Therefore, the well-developed lamellar texture of sample #3 suggests that the sample cooled down slowly, with simultaneous progression of ordering within the Fe-rich isocubanite phase. Meanwhile, the composition of the Fe-rich isocubanite in sample #2 was similar to that of the bulk composition of sample #4; however, the disordered solid solution may have been quenched.

Implications for the geochemical studies of seafloor hydrothermal deposits

The magnetic transition at approximately 100 K is a common feature of isocubanite, at least with an Fe-rich composition. Using low-temperature magnetometry, rapid and non-destructive identification of isocubanite is possible before preparing polished sections for optical and electric microscopy. Isocubanite is considered a mineral specific to young hydrothermal systems (e.g., Mozgova et al. 2005), and magnetometry is expected to be useful for characterizing samples. Magnetic measurements are highly sensitive and can detect trace magnetic minerals that are difficult to detect using other methods, such as powder XRD analysis.

The results of the present study demonstrate that the basic magnetic properties measured in the laboratory are correlated with the microtexture, such as the presence/absence of lamellae and the Cu/Fe ratio of the Fe-rich isocubanite phase. Although the number of samples was very small to confirm a common rule, the results suggest that low-temperature magnetometry can be used as a proxy to estimate the cooling history of isocubanite-bearing ore samples. We did not consider the effect of grain size; however, magnetic properties, including low-temperature remanence, are widely affected by the distribution of particle sizes (e.g., Dunlop and Özdemir 1997). Therefore, information on the mineral texture, such as the degree of grain growth and spacing between lamellae, is included. Moreover, even if the proceeding cation ordering at temperatures below the stable range of the disordered phase is not apparent from textures, such as lamellae, the magnetic properties are expected to provide clues for the development of ordering and, thus, the stage of cooling.

Finally, we emphasize that low-temperature magnetic transitions, which are useful in detecting the mineral, may occur in various metal sulfides. As well known, monoclinic pyrrhotite undergoes the Besnus transition at 30 K (Besnus and Meyer 1964; Dekkers et al. 1989; Rochette et al. 1990). Low-temperature magnetic properties have also been studied in hexagonal pyrrhotite that do not show the Besnus transition (Horng 2018; Horng and Roberts 2018). Troilite undergoes a magnetic transition at around 70 K (Cuda et al. 2011). Greigite (Roberts 1995; Roberts et al. 2011) and smythite (Horng et al. 2020) are magnetic minerals that do not show low-temperature magnetic transitions. Bornite (Jagadeesh et al. 1981) and tetrahedrite (Kitagawa et al. 2015) are reported to show transitions in susceptibility at low temperatures. If the link between the low-temperature magnetism of various metal sulfides and their mineralogical and petrological properties can be clarified in the future, magnetic measurements are expected to become an increasingly powerful method for studying ore formation processes in submarine hydrothermal fields.

Conclusion

We conducted low-temperature magnetometry, optical microscopy, and chemical analysis of isocubanite samples extracted from orebodies collected from submarine hydrothermal fields in the Okinawa Trough and obtained in the laboratory by heating natural cubanite. To the best of our knowledge, the present study is the first to report on the magnetic remanence behavior of mineral isocubanite at low temperatures. In all four samples, a clear magnetic transition occurred at ~100 K, which is consistent with those in a closely related unnamed mineral $CuFe_3S_4$ (np) reported

by Wintenberger et al. (1994). The similarity with np was supported by the results of XRD, electrical resistivity, and Mössbauer spectra of a selected sample. The sharpness of the magnetic transition and strength of low-temperature remanence acquired in the laboratory varied according to the chemical composition and texture, which reflects the local thermal and chemical history of the hydrothermal field. The signal of the magnetic transition at ~ 100 K can be useful for detecting isocubanite by rapid and non-destructive analysis, and the variations in magnetic properties can be used to estimate the local evolutionary history of the hydrothermal field. As magnetic transitions may occur in various ore-forming metal sulfides, low-temperature magnetometry is a potentially powerful technique for studying the development of hydrothermal fields.

Author contributions CK wrote the manuscript. All authors were involved in data interpretation. C.K. and T.H. performed magnetic measurements. CK and KS performed microscopic observations and EPMA analysis. YY performed Mössbauer spectroscopy and prepared Fig. 6. FH measured electrical resistivity and prepared Fig. 7. All authors participated in the discussion of results.

Data availability Data is available upon request.

Declarations

Conflict of interest The authors declare no potential conflicts of interest.

Research involving human participants and/or animals Not applicable.

Informed consent Not applicable.

References

Barbier T, Berthebaud D, Frésard R, Lebedev OI, Guilmeau E, Eyert V, Maignan A (2017) Structural and thermoelectric properties of n-type isocubanite $CuFe_2S_3$. Inorg Chem Front 4:424–432. https://doi.org/10.1039/C6QI00510A

Barbier T, Srinivasan B, Berthebaud D, Eyert V, Frésard R, Macaigne R, Marinel S, Lebedev OI, Guilmeau E, Maignan A (2021) Structural study and evaluation of thermoelectric properties of single-phase isocubanite ($CuFe_2S_3$) synthesized via an ultra-fast efficient microwave radiation technique. Sustain Energy Fuels 5:5804–5813. https://doi.org/10.1039/D1SE01007G

Besnus MJ, Meyer AJP (1964) Nouvelles données expérimentales sur le magnétisme de la pyrrhotine naturelle. In: Proceedings of the International Conference on Magnetism: Nottingham, September, 1964, The Physical Society, London, p 507–511

Butler IB, Fallick AE, Nesbitt RW (1998) Mineralogy, sulphur isotope geochemistry and the development of sulphide structures at the Broken Spur hydrothermal vent site, 29°10′N, Mid-Atlantic Ridge. J Geol Soc 155:773–785. https://doi.org/10.1144/gsjgs.155.5.0773

Cabri LJ (1973) New data on phase relations in the Cu-Fe-S system. Econ Geol 68:443–454. https://doi.org/10.2113/gsecongeo.68.4.443

Caye R, Cervelle B, Cesbron F, Oudin E, Picot P, Pillard F (1988) Isocubanite, a new definition of the cubic polymorph of cubanite $CuFe_2S_3$. Miner Mag 52:509–514. https://doi.org/10.1180/minmag.1988.052.367.10

Cuda J, Kohout T, Tucek J, Haloda J, Filip J, Prucek R, Zboril R (2011) Low-temperature magnetic transition in troilite: a simple marker for highly stoichiometric FeS systems. J Geophys Res 116:B11205. https://doi.org/10.1029/2011JB008232

Dekkers MJ, Mattéi JL, Fillion G, Rochette P (1989) Grain-size dependence of the magnetic behavior of pyrrhotite during its low-temperature transition at 34 K. Geophys Res Lett 16:855–858. https://doi.org/10.1029/GL016i008p00855

Dunlop DJ, Özdemir Ö (1997) Rock magnetism: Fundamentals and frontiers. Cambridge University Press, Cambridge. https://doi.org/10.1017/CBO9780511612794

Fan L, Wang G, Holzheid A, Zoheir B, Shi X (2021) Isocubanite-chalcopyrite intergrowths in the Mid-Atlantic Ridge 26°S hydrothermal vent sulfides. Geochemistry 81:125795. https://doi.org/10.1016/j.chemer.2021.125795

Fleet ME (1970) Refinement of the crystal structure of cubanite and polymorphism of $CuFe_2S_3$. Z Krist Cryst Mater 132:276–287. https://doi.org/10.1524/zkri.1970.132.16.276

Fouquet Y, Pelleter E, Konn C, Chazot G, Dupré S, Alix AS, Chéron S, Donval JP, Guyader V, Etoubleau J, Charlou JL, Labanieh S, Scalabrin C (2018) Volcanic and hydrothermal processes in submarine calderas: the Kulo Lasi example (SW Pacific). Ore Geol Rev 99:314–343. https://doi.org/10.1016/j.oregeorev.2018.06.006

Greenwood NN, Whitfield HJ (1968) Mössbauer effect studies on cubanite ($CuFe_2S_3$) and related iron sulphides. J Chem Soc A 1968:1697–1699. https://doi.org/10.1039/J19680001697

Halbach P, Nakamura KI, Wahsner M, Lange J, Sakai H, Käselitz L, Hansen RD, Yamano M, Post J, Prause B, Seifert R, Michaelis W, Teichmann F, Kinoshita M, Märten A, Ishibashi J, Czerwinski S, Blum N (1989) Probable modern analogue of Kuroko-type massive sulphide deposits in the Okinawa Trough back-arc basin. Nature 338:496–499. https://doi.org/10.1038/338496a0

Horng CS (2018) Unusual magnetic properties of sedimentary pyrrhotite in methane seepage sediments: comparison with metamorphic pyrrhotite and sedimentary greigite. J Geophys Res 123:4601–4617. https://doi.org/10.1002/2017JB015262

Horng CS, Roberts AP (2018) The low-temperature Besnus magnetic transition: signals due to monoclinic and hexagonal pyrrhotite. Geochem Geophys Geosyst 19:3364–3375. https://doi.org/10.1029/2017GC007394

Horng CS, Roberts AP, Chen YH, Shea KS, Chen KH, Lin CH, Zhao X, Chang CK (2020) Magnetic properties of sedimentary smythite (Fe_9S_{11}). J Geophys Res 125:e2019JB018812. https://doi.org/10.1029/2019JB018812

Ishibashi JI, Ikegami F, Tsuji T, Urabe T (2015) Hydrothermal activity in the Okinawa Trough back-arc basin: Geological background and hydrothermal mineralization. In: Ishibashi JI et al (eds) Subseafloor biosphere linked to hydrothermal systems. Springer, New York, pp 337–359. https://doi.org/10.1007/978-4-431-54865-2_27

Jagadeesh MS, Nagarathna HM, Montano PA, Seehra MS (1981) Magnetic and Mössbauer studies of phase transitions and mixed valences in bornite ($Cu_{4.5}Fe_{1.2}S_{4.7}$). Phys Rev B 23:2350–2356. https://doi.org/10.1103/PhysRevB.23.2350

Kaneda H, Shoji T, Takenouchi S (1978) Heating experiments of cubanite. Min Geol 28:71–82. https://doi.org/10.11456/shigenchishitsu1951.28.71. (**in Japanese with English abstract**)

Kase K, Yamamoto M, Shibata T (1990) Copper-rich sulfide deposit near 23°N, Mid-Atlantic Ridge: chemical composition, mineral chemistry, and sulfur isotopes. In: Detrick R, Honnorez J, Bryan WB, Juteau T (eds) Proc ODP, Sci. Results vols 106/109. College Station, TX, p 163–177. https://doi.org/10.2973/odp.proc.sr.106109.139.1990

Kitagawa S, Sekiya T, Araki S, Kobayashi TC, Ishida K, Kambe T, Kimura T, Nishimoto N, Kudo K, Nohara M (2015) Suppression of nonmagnetic insulating state by application of pressure in mineral tetrahedrite $Cu_{12}Sb_4S_{13}$. J Phys Soc Jpn 84:093701. https://doi.org/10.7566/JPSJ.84.093701

Koski RA, Clague DA, Oudin E (1984) Mineralogy and chemistry of massive sulfide deposits from the Juan de Fuca Ridge. Geol Soc Am Bull 95:930–945. https://doi.org/10.1130/0016-7606(1984)95%3c930:MACOMS%3e2.0.CO;2

Kosterov A (2003) Low-temperature magnetization and AC susceptibility of magnetite: effect of thermomagnetic history. Geophys J Int 154:58–71. https://doi.org/10.1046/j.1365-246X.2003.01938.x

Lyubutin IS, Lin CR, Starchikov SS, Siao YJ, Tseng YT (2015) Synthesis, structural and electronic properties of monodispersed self-organized single crystalline nanobricks of isocubanite $CuFe_2S_3$. J Solid State Chem 221:184–190. https://doi.org/10.1016/j.jssc.2014.10.006

Momma K, Izumi F (2011) VESTA 3 for three-dimensional visualization of crystal, volumetric and morphology data. J Appl Cryst 44:1272–1276. https://doi.org/10.1107/S0021889811038970

Moskowitz BM, Frankel RB, Bazylinski DA (1993) Rock magnetic criteria for the detection of biogenic magnetite. Earth Planet Sci Lett 120:283–300. https://doi.org/10.1016/0012-821X(93)90245-5

Mozgova NN, Borodaev YS, Gablina IF, Cherkashev GA, Stepanova TV (2005) Mineral assemblages as indicators of the maturity of oceanic hydrothermal sulfide mounds. Lithol Miner Resour 40:293–319. https://doi.org/10.1007/s10987-005-0030-z

Nozaki T, Nagase T, Takaya Y, Yamasaki T, Otake T, Yonezu K, Ikehata K, Totsuka S, Kitada K, Sanada Y, Yamada Y, Ishibashi JI, Kumagai H, Maeda L, the D/V Chikyu Expedition 909 Scientists (2021) Subseafloor sulphide deposit formed by pumice replacement mineralisation. Sci Rep 11:8809. https://doi.org/10.1038/s41598-021-87050-z

Oudin E, Constantinou G, Thisse Y, Ramboz C (1984) Fluid inclusion and mineralogical evidence for high-temperature saline hydrothermal circulation in the Red Sea metalliferous sediments: preliminary results. Mar Min 5:3–31

Özdemir Ö, Dunlop DJ, Moskowitz BM (1993) The effect of oxidation on the Verwey transition in magnetite. Geophys Res Lett 20:1671–1674. https://doi.org/10.1029/93GL01483

Pearce CI, Pattrick RAD, Vaughan DJ (2006) Electrical and magnetic properties of sulfides. Rev Miner Geochem 61:127–180. https://doi.org/10.2138/rmg.2006.61.3

Putnis A (1977) Electron microscope study of phase transformations in cubanite. Phys Chem Miner 1:335–349. https://doi.org/10.1007/BF00308844

Roberts AP (1995) Magnetic properties of sedimentary greigite (Fe_3S_4). Earth Planet Sci Lett 134:227–236. https://doi.org/10.1016/0012-821X(95)00131-U

Roberts AP, Chang L, Rowan CJ, Horng CS, Florindo F (2011) Magnetic properties of sedimentary greigite (Fe_3S_4): An update. Rev Geophys 49:RG1002. https://doi.org/10.1029/2010RG000336

Rochette P, Fillion G, Mattéi JL, Dekkers MJ (1990) Magnetic transition at 30–34 kelvin in pyrrhotite: Insight into a widespread occurrence of this mineral in rocks. Earth Planet Sci Lett 98:319–328. https://doi.org/10.1016/0012-821X(90)90034-U

Sawada M, Ozima M, Fujiki Y (1962) Magnetic properties of cubanite ($CuFe_2S_3$). J Geomagn Geoelectr 14:107–112. https://doi.org/10.5636/jgg.14.107

Schwartz GM (1927) Intergrowths of chalcopyrite and cubanite; experimental proof of the origin of intergrowths and their bearing on the geologic thermometer. Econ Geol 22:44–61. https://doi.org/10.2113/gsecongeo.22.1.44

Seto Y, Nishio-Hamane D, Nagai T, Sata N (2010) Development of a software suite on X-ray diffraction experiments. Rev High Press Sci Technol 20:269–276. https://doi.org/10.4131/jshpreview.20.269. (**in Japanese with English abstract**)

Sugaki A, Shima H, Kitakaze A, Harada H (1975) Isothermal phase relations in the system Cu-Fe-S under hydrothermal conditions at 350°C and 300°C. Econ Geol 70:806–823. https://doi.org/10.2113/gsecongeo.70.4.806

Szymański JT (1974) The crystal structure of high-temperature $CuFe_2S_3$. Z Krist Cryst Mater 140:240–248. https://doi.org/10.1524/zkri-1974-3-408

Totsuka S (2017) Estimation of subseafloor environment at active hydrothermal fields in Okinawa Trough based on mineralogical and geochemical analysis, Master's Thesis. Kyushu University (not available online)

Wintenberger M, André G, Garcin C, Imbert P, Jéhanno G, Fouquet Y, Wafik A (1994) Intermediate valency, Verwey transition and magnetic structures of a new mineral, $Cu_{1-\epsilon}Fe_{3+\epsilon}S_4$, resulting from the ageing of isocubanite. J Magn Magn Mater 132:31–45. https://doi.org/10.1016/0304-8853(94)90297-6

Yund RA, Kullerud G (1966) Thermal stability of assemblages in the Cu-Fe-S system. J Petrol 7:454–488. https://doi.org/10.1093/petrology/7.3.454

Zierenberg RA, Shanks WC, Bischoff JL (1984) Massive sulfide deposits at 21°N, East Pacific Rise: Chemical composition, stable isotopes, and phase equilibria. Geol Soc Am Bull 95:922–929. https://doi.org/10.1130/0016-7606(1984)95%3c922:MSDANE%3e2.0.CO;2